Hindawi Publishing Corporation
Mathematical Problems in Engineering
Volume 2014, Article ID 748237, 9 pages
http://dx.doi.org/10.1155/2014/748237

Research Article

Integrated Multiobjective Optimal Design for Active Control System Based on Genetic Algorithm

Ma Yong-Quan and Qiu Hong-Xing

College of Civil Engineering, Southeast University, Nanjing 210096, China

Correspondence should be addressed to Ma Yong-Quan; lemon9143@163.com

Received 11 April 2014; Accepted 24 June 2014; Published 14 July 2014

Academic Editor: Haranath Kar

The integrated multiobjective optimal design method for structural active control system is put forward based on improved Pareto multiobjective genetic algorithm, through which the position of actuator is synchronously optimized with active controller. External excitation is simulated by stationary filtered white noise. The root-mean-square (RMS) of structural response and active control force can be achieved by solving Lyapunov equation in the state space. The design of active controller adopts linear quadratic regulator (LQR) control algorithm. Minimum ratio of the maximum RMS of controlled structural displacement divided by the maximum RMS of uncontrolled structural displacement and minimum ratio of the maximum RMS of controlled structural shear divided by the maximum RMS of uncontrolled structural shear, together with minimization of the sum of RMS of active control force, are used as the three objective functions of multiobjective optimization. The optimization process takes the impact of structure and excitation parameter on the optimized results. An eight-storey six-span plane steel frame was used as an emulational example to demonstrate the validity of this optimization method. Results show that the proposed integrated multiobjective optimal design method is simple, efficient, and practical with good universality.

1. Introduction

In the research area of structural active control, optimal design of the control system, especially the position optimization of actuator, is always one of the hottest hot points of research. In nature, the position optimization of actuator is an issue of the optimization of discrete domain [1]. As a result, it is difficult to find the optimal solution through traditional methods [2]. Random search methods, such as simulated annealing algorithm [3, 4] and genetic algorithm [5, 6], are global optimization algorithms which can be used for the issues of discrete optimization. Thus, they are widely applied in the research of position optimization of control devices. However, previous researches have neglected the internal relations between the position optimization of control devices and the controller itself [7], and the optimization processes are always carried out in time domain [8, 9], in which the optimal position of actuator is worked out only based on certain external excitation and optimization rules [10, 11]. Due to the low computing efficiency, researchers tend to apply a simplified shearing series multiparticle model [12, 13]. On such condition, only the optimal storey of actuator instead of its detail plane position can be figured out [14], and the guiding significance of optimized results is inadequate in actual engineering application.

Considering the high cost of initial investment and operation of structural active control system [15–17], the simplistic design may cause horrible waste of resources. In the opinion of the authors of this paper, the security, in the optimal design of active control system, improvement of functions, and economical efficiency of control system should be synthetically considered during its complete lifecycle. For this reason, the optimal design of active control system is essentially a matter of multiobjective optimization with universality. Combining improved Pareto optimal solution theory and genetic algorithm is an effective way for multiobjective optimization.

This paper, based on improved Pareto multiobjective genetic algorithm, puts forward an active control integrated

optimal design method. Compared with the method proposed in previous literatures, the method of optimization design presented in this paper, which can consider the internal relations between the control device's position optimization and the controller itself, can obtain the optimal position of actuator under the condition of the random excitation and stochastic optimization criterion. The optimization process of the method proposed in this paper can be carried out in the frequency domain, so that the computational efficiency is very high, which is applicable to the complex plane model's optimization of active control system, and can obtain the optimal layout position of actuator. In the meanwhile, this has important reference value for the practical application in engineering.

In order to improve computing efficiency, the optimization process is carried out in frequency domain, the random seismic excitation is simulated by stationary filtered white noise. The variance of structural response and active control force can be worked out by obtaining the solution of Lyapunov equation of the structure under stationary filtered white noise in the state space. The design of active controller adopts linear quadratic regulator (LQR) controlling algorithm. Minimization of the ratio between the maximum root-mean-square (RMS) of controlled structural displacement and the maximum RMS of uncontrolled structural displacement and minimization of the ration between the maximum RMS of controlled structural shear and the maximum RMS of uncontrolled structural shear, together with minimization of the sum of RMS of active control force, are used as the three objective functions of multiobjective optimization. At the end, this paper takes a plane frame structure as an example to certify the effectiveness of proposed active control integrated multiobjective optimization design method.

2. Solving the Random Response Based on Lyapunov Equation

2.1. Variance of Uncontrolled Structural Response. The structural dynamic equation of n-particle model excited by earthquake acceleration $\ddot{\mathbf{x}}_g(t)$ is described as follows:

$$\mathbf{M}\ddot{\mathbf{x}}(t) + \mathbf{C}\dot{\mathbf{x}}(t) + \mathbf{K}\mathbf{x}(t) = -\mathbf{M}\boldsymbol{\mu}\ddot{\mathbf{x}}_g(t), \tag{1}$$

where $\mathbf{M}$, $\mathbf{C}$, and $\mathbf{K}$ are the structural mass matrix, damping matrix, and stiffness matrix, respectively; $\mathbf{x}(t)$, $\dot{\mathbf{x}}(t)$, and $\ddot{\mathbf{x}}(t)$ are the structural displacement vector, velocity vector, and acceleration vector, respectively; $\boldsymbol{\mu}$ is the unit column vector.

The state equation of formula (1) can be written as

$$\dot{\mathbf{Y}} = \mathbf{H}\mathbf{Y} + \mathbf{B}\ddot{\mathbf{x}}_g, \tag{2}$$

$$\mathbf{Z} = \mathbf{A}\mathbf{Y} + \mathbf{L}\ddot{\mathbf{x}}_g, \tag{3}$$

where $\mathbf{H} = \begin{bmatrix} \mathbf{0}_{n\times n} & \mathbf{I}_{n\times n} \\ -\text{inv}(\mathbf{M})\times\mathbf{K} & -\text{inv}(\mathbf{M})\times\mathbf{C} \end{bmatrix}$, $\mathbf{B} = \begin{bmatrix} \mathbf{0}_{n\times 1} \\ -\mathbf{I}_{n\times 1} \end{bmatrix}$, and $\mathbf{Y} = \begin{bmatrix} \mathbf{x} \\ \dot{\mathbf{x}} \end{bmatrix}$ are structural state vectors; $\mathbf{Z}$ is the output vector; $\mathbf{I}$ and $\mathbf{0}$ are identity matrix and zero matrix, respectively, and the subscript is the dimensions corresponding to the matrix.

The Clough-Penzien spectrum [18] of filtered white noise is used to simulate the input earthquake acceleration $\ddot{\mathbf{x}}_g(t)$, and it can be presented by state equation as follows:

$$\dot{\mathbf{Y}}_s = \mathbf{H}_s\mathbf{Y}_s + \mathbf{D}_s\mathbf{S}_0 \tag{4}$$

$$\mathbf{Z}_s = \mathbf{A}_s\mathbf{S}_0, \tag{5}$$

where $\mathbf{Y}_s = \begin{bmatrix} \mathbf{x}_g \\ \dot{\mathbf{Y}}_g \end{bmatrix}$, $\mathbf{H}_s = \begin{bmatrix} 0 & 1 \\ -\omega_g^2 & -2\xi_g\omega_g \end{bmatrix}$, $\mathbf{D}_s = \begin{bmatrix} 0 \\ -1 \end{bmatrix}$, and $\mathbf{A}_s = \begin{bmatrix} -\omega_g^2 \\ -2\xi_g\omega_g \end{bmatrix}^T$; ω_g and ξ_g are the predominant frequency and damping ratio of foundation soil, respectively; $\mathbf{S}_0$ refers to the input white noise.

The state equation of earthquake input-structural model can be obtained as follows by combining formulas (2) and (4) as well as formulas (3) and (5):

$$\dot{\mathbf{Y}}_\tau = \mathbf{H}_\tau\mathbf{Y}_\tau + \mathbf{B}_\tau\mathbf{S}_0, \tag{6}$$

$$\mathbf{Z}_\tau = \mathbf{A}_\tau\mathbf{Y}_\tau + \mathbf{L}_\tau\mathbf{S}_0, \tag{7}$$

where $\mathbf{H}_\tau = \begin{bmatrix} \mathbf{H} & \mathbf{B}\mathbf{A}_s \\ \mathbf{0}_{2\times 2n} & \mathbf{H}_s \end{bmatrix}$, $\mathbf{B}_\tau = \begin{bmatrix} \mathbf{0}_{2n\times 1} \\ \mathbf{B}_s \end{bmatrix}$, $\mathbf{A}_s = \begin{bmatrix} \mathbf{A} & \mathbf{L}\mathbf{A}_s \\ \mathbf{0}_{1\times 2n} & \mathbf{A}_s \end{bmatrix}$, $\mathbf{L}_\tau = \mathbf{0}_{(n_z+1)\times 1}$, and the extended state vector $\mathbf{Y}_\tau = \begin{bmatrix} \mathbf{Y} \\ \mathbf{Y}_s \end{bmatrix}$.

The solution of differential equation (6) is

$$\begin{aligned} \mathbf{Y}_\tau(t) = {} & \exp\left(\mathbf{H}_\tau(t-t_0)\right)\mathbf{Y}_{\tau 0} \\ & + \int_{t_0}^{t} \exp\left(\mathbf{H}_\tau(t-T)\right)\mathbf{B}_\tau\mathbf{S}_0(T)\,dT, \end{aligned} \tag{8}$$

where $\mathbf{Y}_{\tau 0}$ is the initial condition when $t = t_0$; $\exp(\mathbf{H}_\tau t)$ is the general solution of first-order equation; the integral term in the right side of the formula above is a particular solution of the equation. For convenience, given $\mathbf{Y}_{\tau 0} = \mathbf{0}$, the formula above can be rewritten as

$$\mathbf{Y}_\tau(t) = \int_{t_0}^{t} \exp\left(\mathbf{H}_\tau(t-T)\right)\mathbf{B}_\tau\mathbf{S}_0(T)\,dT. \tag{9}$$

The related functional matrix of structural response can be calculated through the formula above, and its expression is given as follows:

$$\begin{aligned} & \mathbf{R}_{\mathbf{Y}_\tau\mathbf{Y}_\tau}(t_1, t_2) \\ & = E\left[\mathbf{Y}_\tau(t_1)\,\mathbf{Y}_\tau^T(t_2)\right] \\ & = \int_{t_0}^{t_1}\int_{t_0}^{t_2} \exp\left(\mathbf{H}_\tau(t_1-T_1)\right)\mathbf{B}_\tau E\left[\mathbf{S}_0(T_1)\,\mathbf{S}_0^\tau(T_2)\right] \\ & \qquad \times \mathbf{B}_\tau^T \exp\left(\mathbf{H}_\tau^T(t_2-T_2)\right)dT_1dT_2. \end{aligned} \tag{10}$$

In the formula above, the variance matrix of input excitation is defined as follows:

$$E\left[\mathbf{S}_0(T_1)\,\mathbf{S}_0^\tau(T_2)\right] = 2\pi\mathbf{P}_0\delta(t_2-t_1) = \mathbf{P}_s\delta(t_2-t_1). \tag{11}$$

If we plug the formula above into formula (10) and take the integral property of function δ into account, formula (10) can be transformed into

$$\mathbf{R}_{\mathbf{Y}_\tau \mathbf{Y}_\tau}(t_1, t_2) = \int_{t_0}^{t_1} \exp\left(\mathbf{H}_\tau (t_1 - T_1)\right) \mathbf{B}_\tau \mathbf{P}_s \mathbf{B}_\tau^T \exp\left(\mathbf{H}_\tau^T (t_2 - T_2)\right) dT_1. \tag{12}$$

Provided that $t_2 = t_1 = t$, the variance matrix $\mathbf{B}_{\mathbf{Y}_\tau}$ of response is

$$\begin{aligned}\mathbf{B}_{\mathbf{Y}_\tau} &= \int_{t_0}^{t} \exp\left(\mathbf{H}_\tau (t - T)\right) \mathbf{B}_\tau \mathbf{P}_s \mathbf{B}_\tau^T \exp\left(\mathbf{H}_\tau^T (t - T)\right) dT \\ &= \exp\left(\mathbf{H}_\tau t\right) \cdot \left(\int_{t_0}^{t} \exp\left(-\mathbf{H}_\tau T\right) \mathbf{B}_\tau \mathbf{P}_s \mathbf{B}_\tau^T \exp\left(-\mathbf{H}_\tau^T T\right) dT \right) \exp\left(\mathbf{H}_\tau^T t\right).\end{aligned} \tag{13}$$

Taking the derivative of time t on both sides of the formula above, the result is

$$\frac{d\mathbf{B}_{\mathbf{Y}_\tau}}{dt} = \mathbf{H}_\tau \mathbf{B}_{\mathbf{Y}_\tau}(t) + \mathbf{B}_{\mathbf{Y}_\tau}(t) \mathbf{H}_\tau^T + \mathbf{B}_\tau \mathbf{P}_s \mathbf{B}_\tau^T, \tag{14}$$

where formula (14) is called Lyapunov equation [19] that describes the property of response variance $\mathbf{B}_{\mathbf{Y}_\tau}(t)$. The response maintains stability, and variance is irrelevant to time in a steady situation. At this point, formula (14) can be transformed into

$$\mathbf{H}_\tau \mathbf{B}_{\mathbf{Y}_\tau} + \mathbf{B}_{\mathbf{Y}_\tau} \mathbf{H}_\tau^T = -\mathbf{B}_\tau 2\pi \mathbf{P}_0(S) \mathbf{B}_\tau^T. \tag{15}$$

Variance $\mathbf{B}_{\mathbf{Y}_\tau}(t)$ of state vector $\mathbf{Y}_\tau$ can be obtained by solving the formula above and the variance of output vector $\mathbf{Z}_\tau$ is

$$\mathbf{B}_{\mathbf{Z}_\tau} = \mathbf{A}_\tau \mathbf{B}_{\mathbf{Y}_\tau} \mathbf{A}_\tau^T + \mathbf{L}_\tau \mathbf{P}_0(S) \mathbf{L}_\tau^T. \tag{16}$$

2.2. Variance of Both Controlled Structural Response and Control Force. The structural dynamic equation of n-particle model installed with actuators excited by earthquake acceleration $\ddot{\mathbf{x}}_g(t)$ can be expressed as

$$\mathbf{M}\ddot{\mathbf{x}}(t) + \mathbf{C}\dot{\mathbf{x}}(t) + \mathbf{K}\mathbf{x}(t) = -\mathbf{M}\boldsymbol{\mu}\ddot{\mathbf{x}}_g(t) + \mathbf{N}\mathbf{U}_b. \tag{17}$$

In this formula, $\mathbf{N}$ is the position matrix of control force; $\mathbf{U}_b$ refers to active control force. The following extended state equation can also be achieved according to the procedures in Section 2.1:

$$\begin{aligned}\dot{\mathbf{Y}}_\tau &= \mathbf{H}_\tau \mathbf{Y}_\tau + \mathbf{B}_\tau \mathbf{S}_0 + \mathbf{D}_m \mathbf{U}_b, \\ \mathbf{Z}_\tau &= \mathbf{A}_\tau \mathbf{Y}_\tau + \mathbf{L}_\tau \mathbf{S}_0 + \boldsymbol{\Lambda}_\tau \mathbf{U}_b, \\ \mathbf{Z}_m &= \mathbf{A}_m \mathbf{Y}_\tau + \mathbf{L}_m \mathbf{S}_0 + \boldsymbol{\Lambda}_m \mathbf{U}_b.\end{aligned} \tag{18}$$

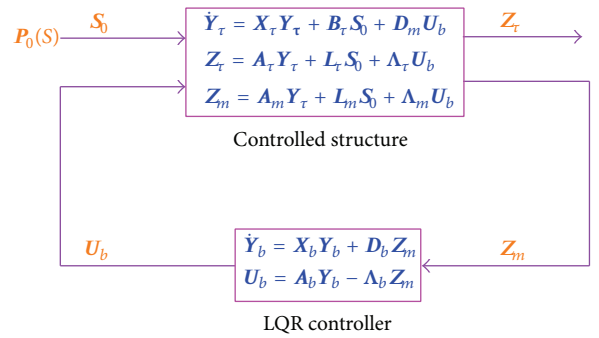

FIGURE 1: Block diagram of stationary filtered white noise-controlled structure-controller.

Optimal feedback gain matrix Q_b is designed using LQR controller [20] so as to obtain expected optimal active control force $\mathbf{U}_b$. And its quadratic objective function is expressed with the following form:

$$\mathbf{V} = \int_0^\infty \left\{ \mathbf{Z}_Y^T \mathbf{G} \mathbf{Z}_Y + \mathbf{U}_b^T \mathbf{J} \mathbf{U}_b \right\} dt, \tag{19}$$

where $\mathbf{Z}_Y$ means control objective vector of the system; $\mathbf{G}$ and $\mathbf{J}$ are the weight matrixes weighing the structural response and active control force, respectively.

The controller design and state estimation are treated separately in accordance with separation principle [21], and optimal control law is determined based on linear quadratic optimal control theory [22] as follows:

$$\mathbf{U}_b = -\boldsymbol{\Omega}_b \mathbf{Y}_b. \tag{20}$$

In this formula, $\boldsymbol{\Omega}_b$ is the full state feedback gain matrix; $\mathbf{Y}_b$ refers to the system state vector estimated based on Kalman filter [23], and it can be expressed as

$$\dot{\mathbf{Y}}_b = \mathbf{H}_\tau \mathbf{Y}_b + \mathbf{D}_\tau \mathbf{U}_b + \boldsymbol{\mu}_b \left(\mathbf{Z}_m - \mathbf{A}_m \mathbf{Y}_b - \boldsymbol{\Lambda}_m \mathbf{U}_b \right), \tag{21}$$

where $\boldsymbol{\mu}_b$ is observer gain matrix and $\mathbf{Z}_m$ means measured response. System state is estimated through measuring acceleration in this paper. Finally, the LQR controller can be described with the following state equation:

$$\begin{aligned}\dot{\mathbf{Y}}_b &= \mathbf{H}_b \mathbf{Y}_b + \mathbf{D}_b \mathbf{Z}_m, \\ \mathbf{U}_b &= \mathbf{A}_b \mathbf{Y}_b - \boldsymbol{\Lambda}_b \mathbf{Z}_m,\end{aligned} \tag{22}$$

where $\mathbf{H}_b = \mathbf{H}_\tau - \mathbf{D}_\tau \boldsymbol{\Omega}_b - \boldsymbol{\mu}_b \mathbf{A}_m + \boldsymbol{\mu}_b \boldsymbol{\Lambda}_m \boldsymbol{\Omega}_b$, $\mathbf{D}_b = \boldsymbol{\mu}_b$, $\mathbf{A}_b = -\boldsymbol{\Omega}_b$, and $\boldsymbol{\Lambda}_b = 0$.

Figure 1 shows the block diagram of filtered white noise-controlled structure-LQR controller.

An extended state equation can be obtained through expanding controlled structure, LQR controller, and filtered white noise into a state equation, which is expressed as

$$\begin{aligned}\dot{\mathbf{Y}}_d &= \mathbf{H}_d \mathbf{Y}_d + \mathbf{D}_d \begin{bmatrix} \mathbf{S}_0 \\ \mathbf{U}_b \end{bmatrix}, \\ \mathbf{Z}_\tau &= \mathbf{A}_d \mathbf{Y}_d - \boldsymbol{\Lambda}_d \begin{bmatrix} \mathbf{S}_0 \\ \mathbf{U}_b \end{bmatrix}.\end{aligned} \tag{23}$$

In this formula, $\mathbf{Y}_d = \begin{bmatrix} \mathbf{Y}^T \\ \mathbf{Y}_s^T \\ \mathbf{Y}_b^T \end{bmatrix}$ refers to the system state; $\mathbf{H}_d$, $\mathbf{D}_b$, $\mathbf{A}_d$, and $\mathbf{\Lambda}_d$ represent the coefficient matrixes, and they can be obtained by using "feedback" command in MATLAB.

Similarly, the variances of both the controlled structure response and the control force under stationary random excitation can be worked out. The peak control force needed in actual engineering application can be figured out conveniently through RMS and peak factor.

3. The Definition of Optimization Principle

Considering that the maximum output force of actuator is limited by its physical conditions in actual engineering application [24], the paper makes an assumption that the RMS control force meets the following constraints:

$$\max\left\{W_{\mathbf{U}^i_{\text{active}}}\right\} \le W_{\mathbf{U}_{\text{permit}}}. \tag{24}$$

In this formula, $W_{\mathbf{U}_{\text{permit}}}$ is the allowed maximum RMS of active control force, and $W_{\mathbf{U}^i_{\text{active}}}$ is the RMS of active control force generated by the ith actuator.

The previous constraints can be treated with penalty function method, and the definition of optimized objective function is

$$\begin{aligned}
\nabla_1 &= \frac{\max_j\left\{W_{x_j^k}\right\}}{\max_j\left\{W_{x_j^{wk}}\right\}} + \eta \times \max\left[0, \frac{\max\left\{W_{\mathbf{U}^j_{\text{permit}}}\right\}}{W_{\mathbf{U}_{\text{permit}}}} - 1\right], \\
\nabla_2 &= \frac{\max_j\left\{W_{Q_j^k}\right\}}{\max_j\left\{W_{Q_j^{wk}}\right\}} + \eta \times \max\left[0, \frac{\max\left\{W_{\mathbf{U}^j_{\text{permit}}}\right\}}{W_{\mathbf{U}_{\text{permit}}}} - 1\right], \\
\nabla_3 &= \sum_{j=1}^{m} W_{\mathbf{U}^j_{\text{active}}} + \eta \times \max\left[0, \frac{\max\left\{W_{\mathbf{U}^j_{\text{permit}}}\right\}}{W_{\mathbf{U}_{\text{permit}}}} - 1\right].
\end{aligned} \tag{25}$$

In the formula, $W_{x_j^k}$ and $W_{Q_j^k}$ are the RMS of both lateral relative displacement and base shear on the jth storey of controlled structure, respectively; $W_{x_j^{wk}}$ and $W_{Q_j^{wk}}$ are the RMS of both lateral relative displacement and base shear on the jth storey of uncontrolled structure, respectively; m refers to the number of actuators; ∇_1 represents the ratio between maximum RMS of lateral relative displacements of both controlled structure and uncontrolled structure; ∇_2 means the ratio between maximum RMS of base shears of both controlled structure and uncontrolled structure; ∇_3 refers to the sum of RMS of active control force. Constraints are taken into account in the second item; η represents penalty factor which is always expressed as a large constant. In the event that the constraints are satisfied, the value of this item is zero. Contrarily, the value of objective function is big while the possibility that it is chosen into next generation is small so as to inflict punishment on this individual. During the optimization process, the closed-loop stability of the system should be guaranteed; otherwise ∇_1, ∇_2, and ∇_3 will be assigned with bigger values as a punishment to the individual.

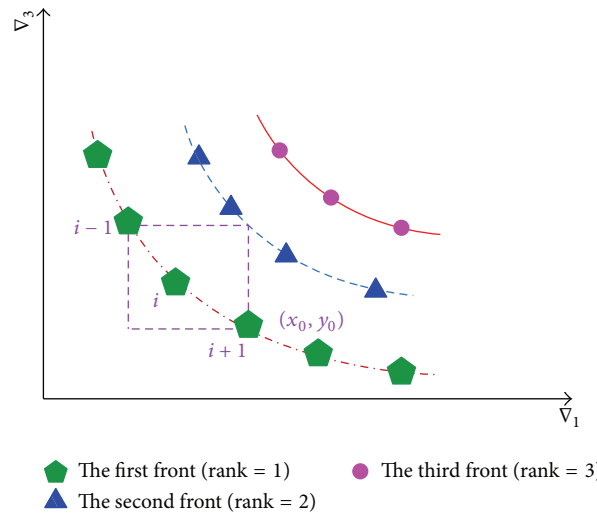

Figure 2: Pareto ordering of two objectives.

4. Improved Multiobjective Genetic Algorithm Based on Pareto Theory

In this paper, improved multiobjective genetic algorithm based on Pareto optimal solution [25] is adopted to make multiobjective integrated optimal design of active control system. In order to obtain a better understanding of this algorithm, three definitions are introduced as follows.

4.1. Pareto Optimal Solution. The issues of multiobjective optimization above can be expressed as minimized objective function vector, which is expressed as

$$\min \nabla(\mathbf{y}) = \{\nabla_1(\mathbf{y}), \nabla_2(\mathbf{y}), \nabla_3(\mathbf{y})\}. \tag{26}$$

In this formula, $\mathbf{y}$ is the decision variable (refer to the positions of actuator and the design parameters of controller), $\mho$ is the decision variable space, Ω refers to objective function space, and $\Omega \in \mathbb{R}^3$.

Define optimal solution $\mathbf{y}^* \in \mho$. And given that there is at least one $r \in \mathbf{X}$ where $\mathbf{X} = \{1, 2, 3\}$,

$$\nabla_r(\mathbf{y}) > \nabla_r(\mathbf{y}^*), \tag{27}$$

where $\mathbf{y}^* \in \mho$ is the Pareto optimal solution. Its manifestation in objective function space is Pareto optimal boundary (known as P optimal frontier curve). As illustrated in Figure 2, Pareto optimal boundary is the curve made up by individuals whose Rank = 1.

4.2. Dominance Relation. Given that λ and ϕ are any two different individuals of the evolving group, the two following conditions should be satisfied if λ dominates ϕ:

(i) for all the subobjectives, λ is not inferior to ϕ; namely, $\nabla_r(\lambda) \le \nabla_r(\phi)$ is always true when $\forall r \in \mathbf{X}$;

(ii) there should be at least one subobjective that makes λ superior to ϕ. Namely, $\nabla_h(\lambda) < \nabla_h(\phi)$ is true when $\exists h \in \{1, 2, 3\}$.

According to the definition of domination, it is easy to find out that the individuals on optimal boundary are not dominated. Provided that its boundary set sequence number is 1 (Rank = 1), the boundary set sequence numbers of other individuals are defined as the numbers of individuals dominating it plus 1. As illustrated in Figure 2, the two subobjectives ∇_1 and ∇_3 form Pareto optimal curve and the three objectives make up an optimal surface. This curve divides objective function space into two parts, the upper space of which is feasible region and the lower space is infeasible region. As illustrated in Figure 2, for the curve coordinate (x_0, y_0), when the control effect to lateral displacement is $1 - x_0$, the corresponding minimum (optimal) control force is y_0, and such control effect cannot be realized if the force is lower than minimum control force.

4.3. Crowding Distance. In the event that sequence numbers of boundary set are equal, the pros and cons of individuals are represented by clustering distance. As illustrated in Figure 2, for two subobjectives ∇_1 and ∇_3, the clustering distance of individual i is the sum of length and width of the dashed quadrangle in the figure. The crowding distance $\widetilde{L}(i)$ of individual i can be defined as

$$\begin{aligned}\widetilde{L}(i) = {} & \left(\widetilde{Q}(i+1)\cdot\nabla_1 - \widetilde{Q}(i-1)\cdot\nabla_1\right) \\ & + \left(\widetilde{Q}(i+1)\cdot\nabla_2 - \widetilde{Q}(i-1)\cdot\nabla_2\right),\end{aligned} \tag{28}$$

where $\widetilde{Q}(i)\cdot\nabla_r$ represents the function value of individual i on the rth subobjective. When there are k subobjectives, (28) can be reexpressed as

$$\widetilde{L}(i) = \sum_{r=1}^{k}\left(\widetilde{Q}(i+1)\cdot\nabla_r - \widetilde{Q}(i-1)\cdot\nabla_r\right). \tag{29}$$

Reference [26] puts forward multiobjective optimal algorithm (NSGA-II); however, this optimal algorithm NSGA-II, when facing the complex optimization problems, has relatively poor computational efficiency and tends towards premature convergence. To overcome the above shortcomings of NSGA-II, an improved multiobjective optimal algorithm is presented in this paper, and the partial ordering relation is defined as follows: during the generation process of new groups, if there are two individuals belonging to different boundary set, the individual with smaller boundary set sequence number is set as priority; if the two boundary sequence numbers are equal, the individual with larger clustering distance is set as priority. The flow diagram of this improved algorithm is shown in Figure 3, and the detailed descriptions are introduced as follows.

(1) Randomly generate initial parent population D_0 and progeny population F_0, the population sizes of D_0 and F_0 are both $\overline{N}$, and define initial time $t = 0$.

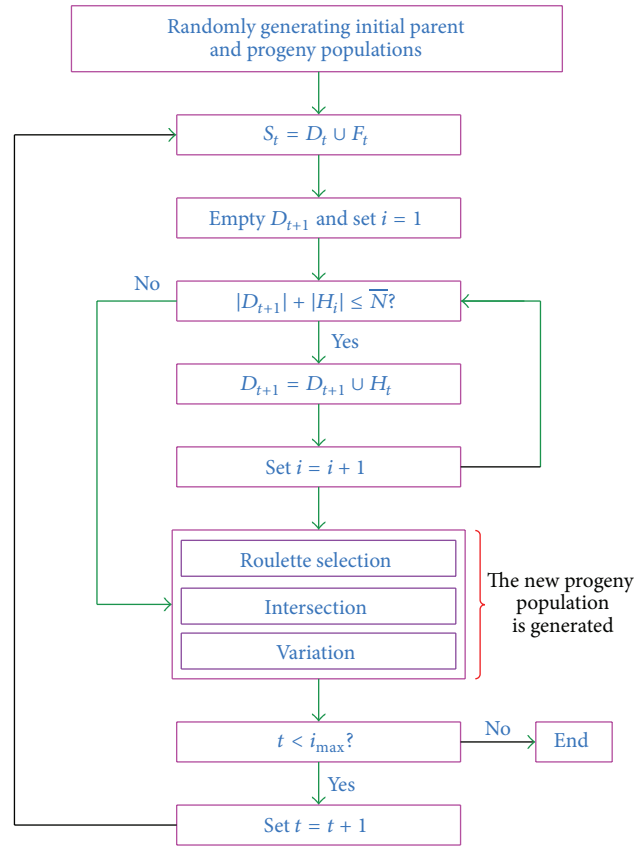

Figure 3: Flow diagram of improved NSGA-II algorithm.

(2) Integrate the two populations (D_t and F_t) into S_t; that is, $S_t = D_t \cup F_t$, and in accordance with the concept of Pareto construct nondomination level surface H of the S_t; that is, $H = \{H_1, H_2, \ldots, H_i\}$.

(3) Empty D_{t+1} (D_{t+1} is the parent population at the moment $t + 1$) and set $i = 1$.

(4) If $|D_{t+1}| + |H_i| \le \overline{N}$, then proceed to Step (5); otherwise, skip to Step (7).

(5) Calculate the clustering distance of individuals in H_i, and add individuals in H_i to the parent population D_{t+1}; that is, $D_{t+1} = D_{t+1} \cup H_t$.

(6) Set $i = i + 1$; return to Step (4).

(7) Perform roulette selection, intersection, and variation operation on D_{t+1} to generate new population F_{t+1}.

(8) If $t < i_{\max}$ ($i_{\max}$ is the maximum evolutionary number of generations), then return to Step (2); otherwise, the algorithm terminates.

5. Simulation Analysis

This paper takes an eight-layer six-span frame structure as an example to examine the effectiveness of new integrated multiobjective optimal algorithm for active control system. As illustrated in Figure 4, numbers from 1~48 are possible positions of the control devices (actuators). Every node of

Table 1: Structural parameters.

Storey number	Column		Beam	
	Bending inertia moment I/m^4	Cross-sectional area A/m^2	Bending inertia moment I/m^4	Cross-sectional area A/m^2
1-2	1.10×10^{-4}	2.20×10^{-2}	8.10×10^{-4}	2.20×10^{-2}
3-4	1.00×10^{-4}	1.90×10^{-2}	7.60×10^{-4}	1.90×10^{-2}
5-6	0.85×10^{-4}	1.60×10^{-2}	6.80×10^{-4}	1.60×10^{-2}
7-8	0.75×10^{-4}	1.40×10^{-2}	6.00×10^{-4}	1.40×10^{-2}

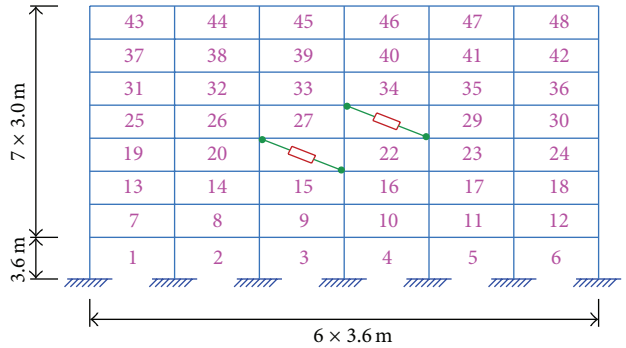

Figure 4: Finite element model of the structure installed with actuators.

this structure has three degrees of freedom, namely, 2 translational motions and 1 rotation. Both the elasticity modulus of the beam and that of the column are $E = 210\,\mathrm{GPa}$, the column density $\rho_c = 7900\,\mathrm{kg{\cdot}m^{-3}}$, and the beam density $\rho_b = 21000\,\mathrm{kg{\cdot}m^{-3}}$. The piezoelectric ceramic actuators (PCA) are used as the active control devices in this paper. The nominal maximum output force of PCA is 1200 kN, and the nominal maximum stroke of PCA is 60 cm. See Table 1 for design parameters of beam and column.

A specific set of reference values of parameters ω_g and ξ_g is given in [27] according to the site classification set forth in China. See Table 2 for parameters of four sorts of sites in the first group of grouping of design earthquake selected in this paper. The measured vector $\mathbf{Z}_m$ takes the horizontal acceleration of each node as its value, and controlled vector $\mathbf{Z}_Y$ takes the horizontal displacement and velocity of each node as its value. The allowed maximum RMS of control force $W_{\mathbf{U}_{\mathrm{permit}}} = 1.2 \times 10^5\,\mathrm{kN}$, and the weight matrixes $\mathbf{G} = 10^{\phi} \times \mathbf{I}_{60\times 60}$ and $\mathbf{J} = \mathbf{I}_{m\times m}$, where m represents the number of actuators whose value is 10. The initial population size is set as 600, and the evolutionary number of generations $\overline{N}_s = 60$. Real coding is applied whose length is 49 dimensions, the first 48 of which are used to identify the position of actuators and the last one is used to identify the weight coefficient ϕ. In simulation analysis, the stiffness ratios of beam to column and site soil feature parameters have different effects on the optimization results of control system.

Optimal frontier curve is illustrated in Figure 5. For intuition and clearance of marking, only 50 individuals are depicted in a two-dimensional view, in which we can observe that the distribution of Pareto solution set is relatively even.

Table 2: Design value of site soil parameters.

Parameter	Site classification			
	I	II	III	IV
ω_g	25.12	17.96	13.95	9.68
ξ_g	0.65	0.71	0.82	0.91

More importantly, improved NSGA-II algorithm is able to provide a Pareto solution set compared to the fact that only one optimal solution can be determined with traditional optimization methods. This algorithm allows decision-makers to make flexible selections of layout schemes according to actual engineering situations, which manifests the superiority of improved active control multiobjective optimal algorithm put forward in this paper.

The actuators' positions and relevant control gains corresponding to some optimal individuals selected from Pareto optimal frontier curve are listed in Table 3 to Table 5, and they correspond to different stiffness ratios of beam to column and the site classifications. By comparing the optimized results shown in Tables 3 and 4, we will discover that site classifications have little impact on the optimized results of actuators' positions if there is little difference between seismic reduction effect of displacement and seismic reduction effect of shear ($1 - \nabla_1$ and $1 - \nabla_2$, resp.), which means the genetic algorithm has strong robustness. As illustrated in Figure 5 and Table 3 to Table 5, when stiffness ratio of beam to column $k_{\mathrm{bc}} = 0.45$, the sum of RMS of control force (∇_3) is a little smaller than that when $k_{\mathrm{bc}} = 4.5$, and the ∇_3 in site classification I is a little larger than that in site classification III. This is mainly caused by the changes of both structural dynamic characteristics and external excitation parameters. The sum of control force increases gradually as the control effect improves. Serial number 1 in Table 3 to Table 5 also indicates that actuators should be deployed on every storey so as to obtain good control effect and that most devices need to be deployed on the two bottom storeys. When the preset control effect declines to a certain range (which corresponds to Serial numbers 2 and three in Table 3 to Table 5), the optimal position of the actuator remains almost still, and active control effect is connected only with control gain, which can be achieved by adjusting weight matrix. The fourth row (Serial number 4) in Table 3 to Table 5 shows the results when actuators are deployed on three bottom storeys according to experience on condition that the weight matrix

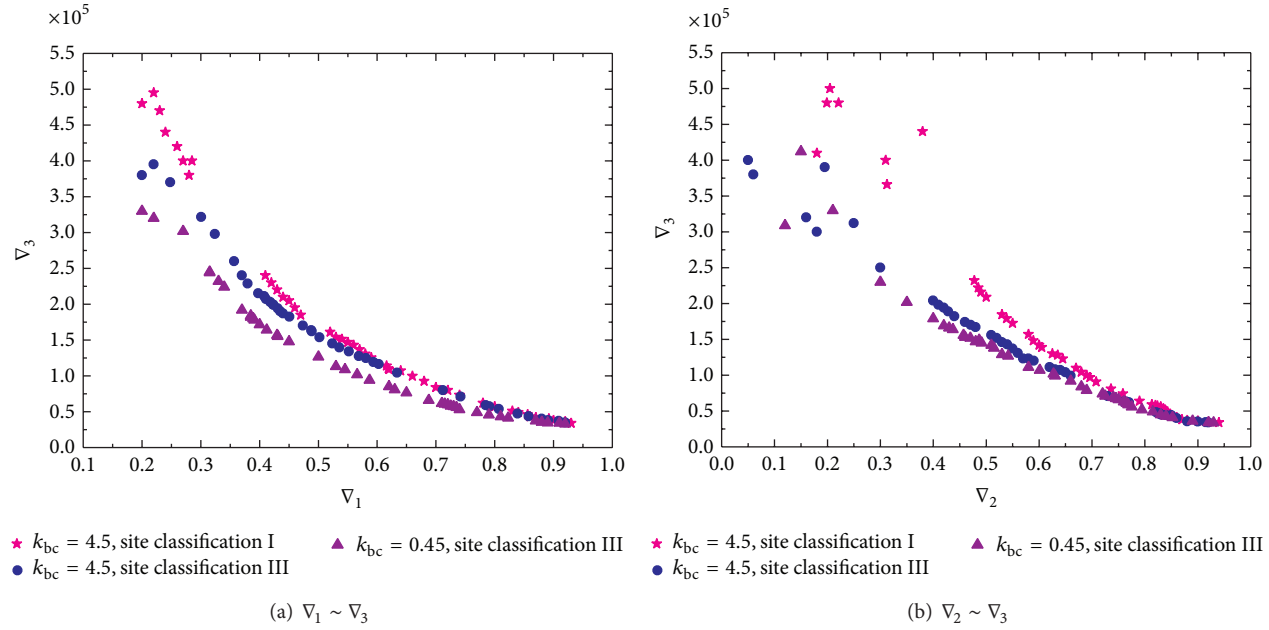

(a) $\nabla_1 \sim \nabla_3$ (b) $\nabla_2 \sim \nabla_3$

Figure 5: Optimal frontier curve of Pareto.

Table 3: Optimized results of site classification I when linear stiffness ratio of beam to column is 4.5.

Serial number	Position of the actuator	∇_1	∇_2	∇_3/kN	ϕ
1	1, 2, 6, 7, 9, 12, 27, 33, 39, 43, 45, 48	0.23	0.37	481	$10^{9.89}$
2	7, 12, 25, 36, 37, 42, 43, 44, 45, 46, 47, 48	0.48	0.54	193	$10^{8.48}$
3	4, 12, 26, 35, 38, 41, 43, 44, 45, 46, 47, 48	0.69	0.73	92	$10^{7.75}$
4	1, 2, 4, 5, 6, 7, 8, 9, 11, 12, 13, 15	0.26	0.36	513	$10^{9.89}$

Table 4: Optimized results of site classification III when linear stiffness ratio of beam to column is 4.5.

Serial number	Position of the actuator	∇_1	∇_2	∇_3/kN	ϕ
1	3, 5, 7, 10, 21, 29, 33, 37, 41, 44, 46, 48	0.22	0.34	405	10^{10}
2	12, 24, 34, 36, 38, 40, 42, 44, 45, 46, 47, 48	0.45	0.47	189	$10^{8.61}$
3	11, 24, 35, 36, 37, 39, 42, 44, 45, 46, 47, 48	0.63	0.65	112	$10^{7.96}$
4	1, 2, 4, 5, 6, 7, 8, 9, 11, 12, 13, 15	0.22	0.35	465	10^{10}

Table 5: Optimized results of site classification III when linear stiffness ratio of beam to column is 0.45.

Serial number	Position of the actuator	∇_1	∇_2	∇_3/kN	ϕ
1	1, 2, 6, 7, 12, 27, 31, 36, 39, 43, 45, 48	0.27	0.35	312	$10^{9.27}$
2	12, 24, 34, 36, 38, 40, 42, 44, 45, 46, 47, 48	0.45	0.52	155	$10^{8.19}$
3	11, 24, 33, 36, 38, 39, 42, 44, 45, 46, 47, 48	0.64	0.70	82	$10^{7.49}$
4	1, 2, 4, 5, 6, 7, 8, 9, 11, 12, 13, 15	0.28	0.37	339	$10^{9.27}$

is the same as that in Serial number 1, which indicates that the system performance index is improved after optimization.

It turns out by the simulation analysis that the optimal controller of active control system is closely related to the position of actuator and that they both are influenced by structural parameters and excitation characteristics. That is why the design of traditional active control system could not obtain optimal seismic reduction effect, because the optimization is done separately into system design optimization and action controller position optimization. As a result, optimal control effect can be obtained only when an integrated design in structure-control system is carried out.

6. Conclusions

Integrated multiobjective optimal design for active control system is presented in this paper by using Pareto optimal solution-based improved multiobjective genetic algorithm and random vibration theory. The conclusion is given as follows.

(1) It is necessary for active control system to make integrated optimal design of the control device position and the controller. Previous optimal design is done

separately into controller design optimization and action controller position optimization, which is the major reason why optimal seismic reduction effect cannot be achieved.

(2) The Pareto optimal solution set based on improved Pareto multiobjective genetic algorithm provides decision-makers with even wider choices, with which they may select corresponding layout schemes in accordance with actual projects. Therefore, it has high project application value.

With simplicity, efficiency, and practicability, integrated multiobjective optimization method for active control system put forward in this paper is expected to have promising engineering application.

Conflict of Interests

The authors declare that there is no conflict of interests regarding the publication of this paper.

Acknowledgments

Financial supports for this research are provided by the National Natural Science Foundation of China (no. 51078077) and the National Science and Technology Pillar Program during the Twelfth Five-Year Plan Period (no. 2012BAJ14B00). These supports are gratefully acknowledged.

References

[1] A. R. Mehrabian and A. Yousefi-Koma, "A novel technique for optimal placement of piezoelectric actuators on smart structures," *Journal of the Franklin Institute*, vol. 348, no. 1, pp. 12–23, 2011.

[2] M. I. Frecker, "Recent advances in optimization of smart structures and actuators," *Journal of Intelligent Material Systems and Structures*, vol. 14, no. 4-5, pp. 207–216, 2003.

[3] V. M. F. Correia, C. M. Mota Soares, and C. A. Mota Soares, "Refined models for the optimal design of adaptive structures using," *Composite Structures*, vol. 54, no. 2-3, pp. 161–167, 2001.

[4] J. M. S. Moita, V. M. F. Correia, P. G. Martins, C. M. M. Soares, and C. A. M. Soares, "Optimal design in vibration control of adaptive structures using a simulated annealing algorithm," *Composite Structures*, vol. 75, no. 1-4, pp. 79–87, 2006.

[5] M. M. Abdullah, A. Richardson, and J. Hanif, "Placement of sensors/actuators on civil structures using genetic algorithms," *Earthquake Engineering and Structural Dynamics*, vol. 30, no. 8, pp. 1167–1184, 2001.

[6] I. Bruant, L. Gallimard, and S. Nikoukar, "Optimal piezoelectric actuator and sensor location for active vibration control, using genetic algorithm," *Journal of Sound and Vibration*, vol. 329, no. 10, pp. 1615–1635, 2010.

[7] D. K. Liu, Y. L. Yang, and Q. S. Li, "Optimum positioning of actuators in tall buildings using genetic algorithm," *Computers and Structures*, vol. 81, no. 32, pp. 2823–2827, 2003.

[8] Q. S. Li, D. K. Liu, J. Tang, N. Zhang, and C. M. Tam, "Combinatorial optimal design of number and positions of actuators in actively controlled structures using genetic algorithms," *Journal of Sound and Vibration*, vol. 270, no. 4-5, pp. 611–624, 2004.

[9] Y. Cha, A. Raich, L. Barroso, and A. Agrawal, "Optimal placement of active control devices and sensors in frame structures using multi-objective genetic algorithms," *Structural Control and Health Monitoring*, vol. 20, no. 1, pp. 16–44, 2013.

[10] Y. J. Cha, A. K. Agrawal, Y. Kim, and A. M. Raich, "Multi-objective genetic algorithms for cost-effective distributions of actuators and sensors in large structures," *Expert Systems with Applications*, vol. 39, no. 9, pp. 7822–7833, 2012.

[11] Y. Cha, Y. Kim, A. M. Raich, and A. K. Agrawal, "Multi-objective optimization for actuator and sensor layouts of actively controlled 3D buildings," *Journal of Vibration and Control*, vol. 19, no. 6, pp. 942–960, 2013.

[12] R. T. Marler and J. S. Arora, "Survey of multi-objective optimization methods for engineering," *Structural and Multidisciplinary Optimization*, vol. 26, no. 6, pp. 369–395, 2004.

[13] P. Tan, S. J. Dyke, A. Richardson, and M. Abdullah, "Integrated device placement and control design in civil structures using genetic algorithms," *Journal of Structural Engineering*, vol. 131, no. 10, pp. 1489–1496, 2005.

[14] Q. S. Li, D. K. Liu, N. Zhang, C. M. Tam, and L. F. Yang, "Multi-level design model and genetic algorithm for structural control system optimization," *Earthquake Engineering and Structural Dynamics*, vol. 30, no. 6, pp. 927–942, 2001.

[15] A. Konak, D. W. Coit, and A. E. Smith, "Multi-objective optimization using genetic algorithms: a tutorial," *Reliability Engineering & System Safety*, vol. 91, no. 9, pp. 992–1007, 2006.

[16] Y. Li, J. Onoda, and K. Minesugi, "Simultaneous optimization of piezoelectric actuator placement and feedback for vibration suppression," *Acta Astronautica*, vol. 50, no. 6, pp. 335–341, 2002.

[17] D. A. Shook, P. N. Roschke, P. Lin, and C. Loh, "GA-optimized fuzzy logic control of a large-scale building for seismic loads," *Engineering Structures*, vol. 30, no. 2, pp. 436–449, 2008.

[18] S. C. Lee and S. W. Han, "Neural-network-based models for generating artificial earthquakes and response spectra," *Computers and Structures*, vol. 80, no. 20-21, pp. 1627–1638, 2002.

[19] C. Chen, "Fuzzy control of interconnected structural systems using the fuzzy Lyapunov method," *Journal of Vibration and Control*, vol. 17, no. 11, pp. 1693–1702, 2011.

[20] A. Bemporad, M. Morari, V. Dua, and E. N. Pistikopoulos, "The explicit linear quadratic regulator for constrained systems," *Automatica*, vol. 38, no. 1, pp. 3–20, 2002.

[21] A. N. Atassi and H. K. Khalil, "A separation principle for the control of a class of nonlinear systems," *IEEE Transactions on Automatic Control*, vol. 46, no. 5, pp. 742–746, 2001.

[22] P. Ignaciuk and A. Bartoszewicz, "Linear-quadratic optimal control strategy for periodic-review inventory systems," *Automatica*, vol. 46, no. 12, pp. 1982–1993, 2010.

[23] Y. Shi and H. Fang, "Kalman filter-based identification for systems with randomly missing measurements in a network environment," *International Journal of Control*, vol. 83, no. 3, pp. 538–551, 2010.

[24] S. Korkmaz, "A review of active structural control: challenges for engineering informatics," *Computers and Structures*, vol. 89, no. 23, pp. 2113–2132, 2011.

[25] K. Deb, M. Mohan, and S. Mishra, "Evaluating the ϵ-domination based multi-objective evolutionary algorithm for a quick computation of Pareto-optimal solutions," *Evolutionary Computation*, vol. 13, no. 4, pp. 501–525, 2005.

[26] K. Deb, A. Pratap, S. Agarwal, and T. Meyarivan, "A fast and elitist multiobjective genetic algorithm: NSGA-II," *IEEE*

Transactions on Evolutionary Computation, vol. 6, no. 2, pp. 182–197, 2002.

[27] S. D. Xue, X. S. Wang, and Z. Cao, "Parameters study on seismic random model based on the new seismic code," *China Civil Engineering Journal*, vol. 36, no. 5, pp. 5–10, 2003.